Underpotentially deposited thallium on silver (111) by *in situ* surface x-ray scattering

Michael F. Toney, Joseph G. Gordon, Mahesh G. Samant, Gary L. Borges, and Owen R. Melroy
IBM Research Division, Almaden Research Center, San Jose, California 95120

Dennis Yee and Larry B. Sorensen
Department of Physics, FM-15, University of Washington, Seattle, Washington 98195
(Received 21 August 1991; revised manuscript received 12 December 1991)

Using *in situ* surface x-ray scattering, we have investigated the atomic structure, the stability, and the dependence of the structure on electrode potential for electrochemically deposited Tl monolayers and bilayers on Ag(111). The layers were formed by underpotential deposition (UPD) at electrode potentials positive of the reversible potential for bulk Tl deposition. At potentials between -475 and -680 mV (versus Ag/AgCl), the Tl deposit forms an incommensurate, hexagonal two-dimensional (2D) monolayer that is compressed relative to bulk Tl by 1.4–3.0% and rotated from the Ag $[01\bar{1}]$ direction by $\Omega = 4°-5°$. The structure of the monolayer does not change over at least 24 h (the longest we waited). From diffraction scans of the Tl Bragg rods, we find that the in-plane and vertical root-mean-square displacement amplitudes are 0.36 ± 0.1 and 0.46 ± 0.1 Å, respectively. The monolayer structure is the same as that of vapor-deposited Tl/Ag(111), and this shows that the interaction between the solvent molecules and the Tl adatoms does not influence the monolayer structure. Since the monolayer has a structure that is about the same as the closest-packed planes of bulk Tl, we deduce that the adatom-adatom interactions are the most important structure-determining forces. The compression of the monolayer (compared to bulk Tl) is explained in terms of effective-medium theory. With decreasing electrode potential, the in-plane spacing between Tl adatoms decreases and this permits a calculation of the 2D compressibility. This decreases with atomic spacing, but has an average value $\kappa_{2D} = 1.54\pm0.10$ Å^2/eV, which is similar to previously measured compressibilities of UPD monolayers and is in reasonable agreement with theoretical estimates. The rotation angle Ω depends on electrode potential and adatom spacing, but irreversibly decreases with potential cycling (which is possibly due to the adsorption of trace impurities). Despite this irreversibility, the dependence of Ω on adatom spacing qualitatively agrees with theory. We have investigated the structure of monolayers where the deposition potential is reached in either an anodic or cathodic scan and found these structures to be identical. This shows that the monolayer is in thermodynamic equilibrium and that the finite width and offset of the peaks in the deposition curves are due to kinetics, the influence of adsorbed anions, and/or substrate heterogeneity. At potentials between the monolayer region and bulk deposition, Tl forms a bilayer and this also has a hexagonal structure that is incommensurate with the Ag(111) substrate. In the bilayer, the compression is 1.0% (compared to bulk Tl) and the rotation from the Ag $[01\bar{1}]$ direction is 3.9°; these are both less than in the monolayer.

I. INTRODUCTION

Underpotential deposition (UPD) is the electrochemical adsorption of one or more metal layers onto a foreign metal substrate at electrode potentials positive of the reversible potential for bulk deposition. The phenomenon of UPD has been intensely investigated over the last 25 years using polycrystalline substrates,[1,2] but in recent years there has been an emphasis on single-crystal substrates. The chemical and electronic properties of UPD layers on such electrodes have been explored with a variety of *in situ* and *ex situ* techniques. Because the use of an *ex situ* technique necessitates emersion of the electrode, which may modify the properties of the adsorbed layer, an *in situ* experimental probe is desirable. *In situ* studies of the electronic and chemical properties have been successfully conducted, but direct determination of the atomic structure has proven elusive. This is largely because standard surface-structural techniques [low-energy electron diffraction (LEED), reflection high-energy electron diffraction (RHEED), ion scattering, etc.] rely on probes that cannot penetrate the liquid layer above an electrode. In contrast, surface x-ray scattering[3,4] and absorption spectroscopy[5,6] are ideally suited for studies of such buried interfaces and substantial progress has been made recently in determining, *in situ*, the atomic structure of solid-liquid interfaces, in general, and UPD layers, in particular.[3–17]

In this paper we describe our results for UPD Tl on Ag(111). This system has been previously investigated by electrochemical[18–23] and *in situ* optical [23–26] methods, and based on these experiments, surface structures have been proposed. However, since these measurements only indirectly probe structure, a definitive determination has not yet been made. Fleischman and Mao[27] performed an *in situ* x-ray experiment of UPD Tl using roughened Ag electrodes (to enhance the signal). However, it is not clear that their proposed surface structure for Tl/Ag(111) can adequately explain their data. (This is described in Sec. VII.)

We have considered Tl/Ag(111) as a prototypical UPD system and have done extensive measurements on this system. In a previous publication,[12] we discussed the spatial modulation in the incommensurate Tl monolayer that is induced by the periodic potential of the substrate, and we showed how this can be measured from the intensity of the x-ray scattering from the Ag substrate (the Ag-crystal truncation rods). Herein, we describe our results for the two-dimensional (2D) atomic structure and the thermodynamic stability of the UPD Tl layers; we also describe the dependence of the UPD monolayer structure on electrode potential and report a preliminary structure for the bilayer (which forms at potentials just positive of bulk deposition). The results of these experiments provide insight into the structure-determining forces for UPD layers deposited on smooth substrates and provide a basis for understanding the optical properties of these layers.[23,24,26]

The remainder of this paper is organized as follows. In Sec. II we outline the experimental details, and in Sec. III we describe the UPD of Tl on Ag(111). Section IV gives a description of the Tl monolayer including (a) our x-ray-scattering results, (b) the atomic structure of the layer, (c) the important interactions that determine this structure, and (d) an explanation of the large compression of the monolayer. Section V addresses the stability of the monolayer and presents data for the structure of monolayers where the deposition potential is reached in either an anodic or cathodic scan. Section VI describes the dependence of the monolayer structure on electrode potential, particularly the near-neighbor spacing (i.e., the compressibility) and the rotation angle. The Tl bilayer structure is briefly described in Sec. VII and Sec. VIII contains a summary and conclusions.

II. EXPERIMENTAL ASPECTS

All our experiments were performed *in situ* (in electrolyte), under potential control, and at room temperature. The electrochemical cell is essentially the same as that used in our previous investigations and has been described elsewhere in detail.[7,8] The only significant difference is the addition of a cylindrical Kapton cap that surrounds the electrode and the polypropylene film that confines the electrolyte. We flow N_2 or Ar gas through this cap to prevent oxidation of the monolayer that would be caused by diffusion of atmospheric O_2 through the polypropylene film. With this arrangement, no changes in the diffraction pattern from the monolayer were observed over a period of about 24 h, which was our longest observation time. The Tl layers were deposited with the cell "inflated" so a relatively thick ($\sim$1-mm) layer of electrolyte covered the Ag(111) electrode. The electrolyte was then partially withdrawn and the surface diffraction data were measured through the thin ($\lesssim$30-μm) layer of electrolyte that remained on the electrode. When the cell is "deflated," there is only a small electrolyte volume ($\sim$12 μl) in contact with the electrode and the diffusion length to the substrate is long. Thus, it is likely that only a small amount of impurities adsorb onto the electrode with the cell deflated.

The electrolyte was $0.1M$ Na_2SO_4 containing $2.5\times10^{-3}M$ Tl_2SO_4 and was prepared from Aldrich ultrapure reagents and "nanopure" (Barnstead), deionized water. All potentials were measured relative to the Ag/AgCl ($3M$ KCl) reference electrode in the diffraction cell. The measured Nernst potential for bulk Tl deposition was -710 mV. The electrode substrates were epitaxially grown Ag thin films that were vapor deposited onto freshly cleaved mica.[7,8] These films grow with the [111] direction perpendicular to the substrate surface and the epitaxy of the films is excellent, with an in-plane mosaic spread of $\simeq0.2°$–$0.3°$. From the radial width of the surface peaks, the surface domain size is calculated to be $\simeq500$ Å.

X-ray data were obtained at the National Synchrotron Light Source beam line X20A.[28] Most data were collected in a grazing-incidence geometry ($\simeq0.8°$ incidence angle), although for the out-of-plane measurements, this condition was relaxed. An incident x-ray energy of 9997 eV (1.240 Å) was selected using a Si(111) double-crystal monochromator. Approximately 5 mrad of x-ray radiation were collected from a bending magnet and focused onto the sample with a torodial mirror. This produced a spot at the sample with vertical and horizontal full widths at half maximum (FWHM) of 0.78 and 1.72 mm, respectively. The incident-beam intensity was monitored by a NaI scintillation detector viewing a Kapton foil, and the incident flux was approximately 2×10^{11} sec.$^{-1}$ The diffracted beam was analyzed with 1-mrad Soller slits and the intensity was measured with a NaI scintillation detector. The acceptance of the diffracted beam out of the scattering plane was defined by slits and was 24 mrad. Since the diffraction from monolayers is extended in a direction perpendicular to the layer, the use of a grazing-incidence geometry results in a good match between the monolayer diffraction and the out-of-plane acceptance. This is the principal advantage of the grazing-incidence geometry. The sample was mounted on a Huber four-circle diffractometer and all data were obtained in the symmetric ($\omega=0$) mode.[29]

It is important to note that, in contrast to many electrochemical experiments (where the data collection is rather quick), these surface x-ray-scattering measurements are time consuming. To obtain a typical data set at a given potential, required at least 2 h, although during experiments to test the stability of the UPD layer, the data-collection time was as long as 24 h.

III. UNDERPOTENTIAL DEPOSITION OF Tl/Ag(111)

Before discussing our x-ray measurements, we first describe the UPD of Tl on Ag(111). UPD layers are often deposited by linearly ramping the electrode potential in a negative (or cathodic) direction from an initial potential that is positive enough that no metal is adsorbed. Figure 1 shows the current flowing to the Ag electrode during such a linear potential ramp (a cyclic voltammogram or CV) for Tl on Ag(111).[18,19] If the adsorbing ion is completely discharged [as for Tl/Ag(111) (Ref. 18)] and kinetic effects are absent, the current flow is proportional to

the derivative of the adsorption isotherm.[30] (See the inset in Fig. 1.) When the potential reached −700 mV (just positive of the Nernst potential for deposition of bulk Tl), the direction of the potential ramp is reversed (anodic scan) and the Tl layers are stripped (or desorbed) from the Ag surface.

The predominant features in Fig. 1 are two sets of large, sharp peaks. The first set occurs at approximately −470 mV (240 mV positive of the Nernst potential), and the peak with negative current results from deposition of Tl, while the positive-current peak is due to stripping. Since the charge associated with deposition (see inset in Fig. 1) is close to that expected for a close-packed monolayer of Tl, this negative-current peak has previously been attributed to the deposition of a monolayer of Tl.[18,23,30] Correspondingly, the second negative-current peak in Fig. 1 is attributed to the deposition of a second layer of Tl on top of the first, forming a bilayer. In the potential range −540 to −680 mV, and Tl monolayer has been reported to be stable for at least 1 h.[18] Our results support this and show that in the potential region between −680 and −500 mV the Tl monolayer is stable for at least 24 h (the longest we waited).

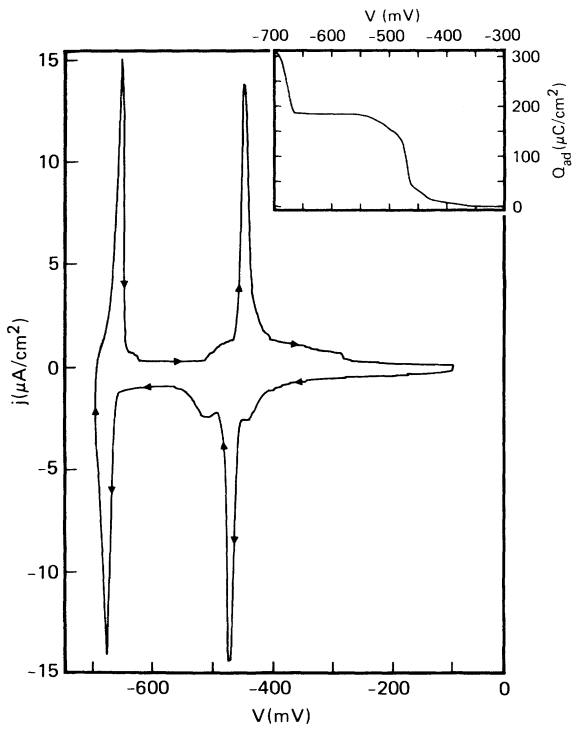

FIG. 1. Cyclic voltammogram (CV, or current-vs-voltage scan) for the deposition of Tl on Ag(111) in $2.5\times10^{-3}M$ Tl_2SO_4 and $0.1M$ Na_2SO_4. The potentials were measured relative to Ag/AgCl ($3M$ KCl) and the Nernst potential for bulk deposition was −710 mV. The arrows indicate the scan directions and the scan rate was 2 mV/sec. The inset shows the adsorption isotherm, which is the integral of the current in the cyclic voltammogram. This is the charge, Q_{ad}, that flows into the electrode during Tl deposition. There is a background current due to processes that do not involve deposition of Tl. This background current was estimated by a linear current that passes through the cyclic voltammogram at $V=-600$ and −180 mV. It has been subtracted from the data in the calculation of Q_{ad}.

IV. MONOLAYER STRUCTURE OF Tl/Ag(111)

A. Surface x-ray-scattering results

We will now discuss our *in situ* x-ray-scattering data for the Tl monolayer. Figure 2 shows the in-plane diffraction pattern for the monolayer determined from our data (such as shown in Fig. 3). In this diffraction pattern, the normal to the substrate is perpendicular to the plane of the paper. The diffraction pattern results from two domains of Tl, which are oriented symmetrically with respect to the Ag($\bar{2}$11) direction. Both domains were observed with equal intensity. The diffraction pattern (Fig. 2) is similar to the LEED pattern that would be observed for Tl/Ag(111), if it were possible to obtain LEED data in an electrolyte.

Figure 3 shows radial and azimuthal diffraction scans of the (10) Bragg rod from the Tl monolayer at −550 mV. In an azimuthal (or rocking) scan, the diffracted intensity is measured along an arc at a constant scattering vector, $Q=(4\pi/\lambda)\sin\theta$, while in a radial scan, the intensity is measured along a radius at constant sample orientation, ϕ. In the radial scan, the intensity is plotted against $Q_{\|}$, the component of the scattering vector parallel to the surface. These data show good signal to background, with peak count rates of about 10 000 counts per second (counts/sec) over a background of 2500 counts/sec. The background is mostly due to scattering from the electrolyte. The azimuthal scan shows peaks at $\phi=\pm4.6°$ from the two rotational domains of the Tl

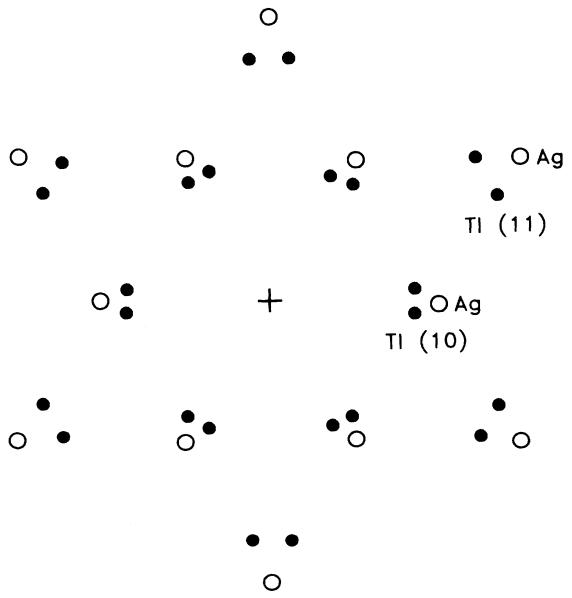

FIG. 2. In-plane x-ray-diffraction pattern ($Q_z=0$) for a monolayer of Tl on Ag(111). The center of the pattern is illustrated with a plus sign, the Ag reflections with open circles, and the Tl reflections with solid circles. There are two observed domains, oriented ±4.6° from the Ag substrate.

monolayer. The diffraction from the two domains is the same (i.e., symmetric about $\phi=0$), but each peak is asymmetric and has a long tail that extends toward $\phi=0$. This is caused by an asymmetric distribution of domains where some domains have a significantly smaller rotation angle than the average.

Scans along the Tl Bragg rods provide information about the atomic correlations perpendicular to the surface and are shown in Fig. 4 for the (10) and (11) Bragg rods. In these rod scans, the diffracted intensity is measured with $\mathbf{Q}_{\parallel}$ held constant, while the component of the scattering vector perpendicular to the substrate surface (Q_z) is varied. In Fig. 2, this corresponds to measuring the intensity along a direction perpendicular to the plane of the paper. The data were obtained by measuring the peak intensity and subtracting the background (which was obtained at azimuthal angles $\pm 1.2°$ from the peak). Since azimuthal scans at different Q_z showed that the azimuthal width did not depend on Q_z, the peak intensity was used in the analysis of the rod scans (rather than the azimuthally integrated intensities). The data in Fig. 4 have been corrected for sample area, Lorentz factor (essentially unity for our case of measuring the peak intensities[31]), the Tl atomic form factor,[32] and the resolution function.

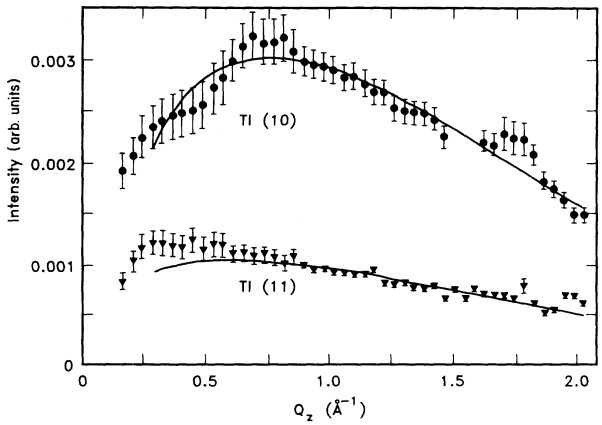

FIG. 4. Rod scans of the Tl (10) and Tl (11) Bragg rods (circles and triangles, respectively) for a layer deposited at -600 mV (vs Ag/AgCl). The data are the measured peak intensities after subtracting off the background and have been corrected for sample area, Lorentz factor, Tl atomic form factor, and resolution function. The solid lines are the best fits to the data with $\sigma_x=0.36\pm0.1$ Å, $\sigma_z=0.46\pm0.1$ Å, and solution thicknesses of 21 and 10 μm for the (10) and (11) rods, respectively.

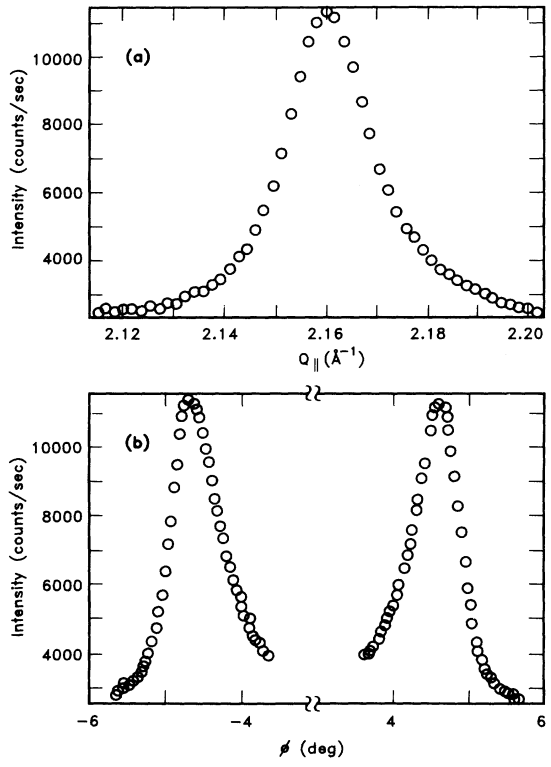

FIG. 3. X-ray diffraction from Tl on Ag(111) for a deposition potential of -550 mV (vs Ag/AgCl). (a) A radial scan of the Tl (10) Bragg rod. In this scan the magnitude of the scattering vector $Q=|\mathbf{Q}|$ was varied, but the aximuthal angle was fixed at $\phi=4.6°$. The azimuthal angle is the angle between Q and the Ag ($\bar{2}11$) direction. (b) An azimuthal angle scan of the Tl (10) Bragg rod at fixed $Q_{\parallel}=2.16$ Å^{-1}. In both scans, the component of the scattering vector perpendicular to the substrate surface is $Q_z=0.15$ Å^{-1}.

The sample-area and resolution-function corrections are described in detail elsewhere.[31] Briefly, the sample-area correction compensates for the variable illumination of the sample with incidence angle and was made using the measured beam shape.[31] The resolution-function correction accounts for the overlap between the surface scattering and the highly anisotropic resolution volume associated with our scattering geometry.[33,34] The anisotropic resolution volume tilts as a scan is made along the Bragg rod, resulting in a decreasing overlap with increasing Q_z. To correct the experimental data for this, we have used the approach described in Ref. 31; this requires a knowledge of the in-plane ($Q_z\simeq 0$) Tl line shapes and the width of the resolution volume out of the scattering plane. This width was determined to be 0.12 Å^{-1},[31] and the in-plane peak shapes were fitted to Lorentzian-squared functions with widths $b=0.0173$ Å^{-1} [for the Tl (10) rod] and $b=0.0211$ Å^{-1} [for the (11) rod].[35]

The rod scans in Fig. 4 vary only slowly with Q_z. This behavior is precisely that expected for the Bragg-rod intensity from a 2D monolayer, where the intensity decreases slowly with increasing Q_z, due the atomic form factor and the Debye-Waller factor. The intensity also decreases at small Q_z, because of x-ray absorption by the electrolyte. The solid lines in Fig. 4 are best fits to the data ($\chi^2=1.35$) with five adjustable parameters: Debye-Waller factors parallel and perpendicular to the surface, an overall scale factor, and thicknesses of the electrolyte layer for the (10) and (11) Bragg rods. We used different solution thicknesses for the (10) and (11) rods, because the clips retaining the substrate result in a nonuniform thickness of the electrolyte layer above the electrode, and the (10) and (11) Bragg rods are observed at different azimuthal orientations of the sample cell and hence

different positions of the clips with respect to the incident and scattered x rays. The use of one uniform thickness worsens the fit slightly (χ^2 increases to 1.7), but does not affect the values given below for the Debye-Waller factors.

The best fit to the data in Fig. 4 yields an in-plane root-mean-square (rms) displacement amplitude of $\sigma_x = 0.36 \pm 0.1$ Å and a vertical rms displacement amplitude of $\sigma_z = 0.46 \pm 0.1$ Å. The ratio of the rod intensities essentially determines σ_x, while σ_z obtains from the decrease in the rod intensities with increasing Q_z. The values of σ_x and σ_z for the UPD monolayer are substantially larger than for bulk Tl ($\sigma_b = 0.14$ Å),[36] as is typically found for adsorbed monolayers and at surfaces.[37] The rms displacement amplitudes contain contributions from both dynamic disorder (vibrations) and static disorder. For an incommensurate monolayer, both dynamic and static disorder are typically larger than their bulk values. The dynamic disorder is larger, because there are fewer near neighbors in the monolayer; while the static disorder tends to be large due to both the presence of more defects and to the vertical buckling and the horizontal displacements that are caused by the modulation included by the substrate (see Sec. IV B). From Eq. (1) of Ref. 12, we calculate that this contribution to σ_x is $2|\mathbf{u}_\mathbf{G}| \simeq 0.08$ Å, where $\mathbf{u}_\mathbf{G}$ is the in-plane amplitude of the substrate-induced modulation with wave vector $\mathbf{G}$.

B. Structure of the monolayer

The diffraction pattern (Fig. 2) together with out-of-plane scans of the Bragg rods show that the Tl layer is a 2D incommensurate, hexagonal monolayer in which the adatoms are closely packed together. This structure is almost the same as that of the close-packed, (00.1) planes of bulk Tl, but the monolayer is compressed compared to the bulk metal. The monolayer domains are rotated about 4°–5° from the Ag [01$\bar{1}$] direction and Fig. 5 shows two schematic representations of the real-space structure of one domain of Tl on Ag(111). The open circles represent atoms of the Ag(111) surface and have a diameter proportional to their nearest-neighbor spacing (2.89 Å). The solid circles represent the Tl adatoms and have a diameter proportional to their average nearest-neighbor spacing $a_{NN} = 3.36$ Å. Figure 5(a) shows the average structure of the Tl monolayer; it ignores the subtle local modulation in near-neighbor positions that results because the adatoms tend to move toward the lowest-energy sites on the substrate.[12] We have previously determined this substrate-induced spatial modulation in the Tl monolayer by measuring the intensity changes along the Ag truncation rods when the monolayer is deposited, and we find that it has an amplitude of 0.03 Å.[12] The structure of the modulated monolayer is shown in Fig. 5(b). The spatial modulation appears as local density increases and decreases and these are apparent in Fig. 5(b) as "overlapping" adatoms and "empty spaces" between adatoms, respectively. These local density changes increase the monolayer elastic energy, but this increase is more than compensated for by the decrease in the adsorbate-substrate interaction energy due to the modulation.

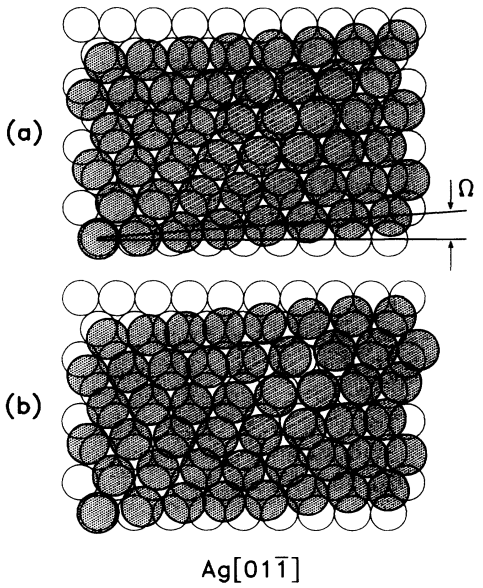

FIG. 5. Schematic real-space representation of one domain of monolayer Tl on Ag(111). The rotation angle between the Ag and Tl lattices is $\Omega = 4.5°$ and the average near-neighbor spacing of the Tl monolayer is 3.36 Å. The open circles represent atoms in the Ag(111) surface and the solid circles represent the Tl atoms; the lower leftmost adatom is arbitrarily positioned above a Ag atom. (a) The (hypothetical) unmodulated or average structure. (b) The modulated monolayer. The adatoms positions are calculated as described in Ref. 12.

The FWHM of the radial scan shown in Fig. 3 is 0.0185 Å^{-1}.[38] This indicates that the domain size of the Tl monolayer is about 300 Å, which is comparable to that observed in our previous measurements of Pb/Ag(111).[7,8] In this estimate of domain size, we have assumed that the peak broadening beyond the resolution is only caused by finite domain size. This is reasonable, since the Tl (11) peaks are only slightly broader than the Tl (10) peaks (by about 20%; see Sec. IV A), and so the inhomogeneous strain is small ($\Delta a_{NN}/a_{NN} \sim 0.3\%$). In addition, the domain size is estimated as $(0.89)2\pi$ over the peak width (FWHM).[39] We note that monolayer peaks have an approximately Lorentzian-squared shape, although we do not attach any physical significance to this.

The Tl peak widths are observed to increase each time the potential is cycled and the cell is inflated. On a "fresh" Ag(111) substrate, the peak width is about 0.015 Å^{-1} (a domain size of $\simeq$370 Å), but as the monolayer is stripped and redeposited (inflating the electrochemical cell for each cycle), the monolayer peak width increases (over about 9 h) to approximately 0.025 Å^{-1} (a domain size of $\simeq$200 Å), and then remains approximately constant. Similarly, the mosaic spread of the monolayer irreversibly increases when the cell is inflated and the potential is cycled; it starts at about 0.4° and increases to 0.8°–0.9°. This shows that the crystalline quality of the Tl monolayer slowly degrades each time the cell is inflated. If the cell is not inflated, the radial width and the mosaic spread of the monolayer do not increase. In addition, even when the cell is inflated and the potential

is cycled, we do not observe a significant increase in the radial width and mosaic spread of the surface diffraction from the Ag substrate (Ag truncation rods); over 30 h, these increase by $\lesssim 10\%$.

The monolayer rotation angle Ω also irreversibly decreases with potential cycling in a manner analogous to the increase in the monolayer peak widths. When the monolayer is stripped and redeposited with the cell inflated, Ω decreases. But if the cell is kept deflated, Ω (and the domain size and mosaic) remain constant. We also observe a dependence of Ω on electrode potential. This and the potential dependence of the near-neighbor spacing are described in Sec. VI. We emphasize that the near-neighbor spacing *does not* show any time dependence.

It seems likely that the same cause accounts for both the loss in crystallite quality of the monolayer and the irreversible decrease of Ω when the cell is inflated. We speculate that this is due to the adsorption of trace amounts of impurities (probably organics) when the electrochemical cell is inflated and the potential cycled. This hypothesis is consistent with our observation that the peak widths of the Ag surface diffraction do not change when the cell is inflated and with the observation [for Kr/Pt(111) in ultrahigh vacuum (UHV)] that small quantities of adsorbed impurities significantly influence the rotation angle.[40] In a previous study of Pb/Ag(111), we did not observe a dependence of the rotation angle on near-neighbor spacing,[9,11] in contrast to the dependence we observe here (see Sec. VI B). It seems likely that this lack of dependence also resulted from impurity adsorption.

C. Structure-determining interactions

The diffraction pattern and 2D structure for the UPD monolayer of Tl/Ag(111) (Figs. 2 and 5) are essentially identical to those of vapor-deposited Tl on Ag(111) near full coverage;[41] however, the compression of the monolayer in the UHV experiments [$(1.2\pm0.6)\%$] is slightly less than for UPD Tl (1.4–3.0 %; see Sec. VII A) and the rotation angle ($\Omega=4.9°\pm0.2°$) is slightly larger. This structural similarity is consistent with previous work where we have observed that the 2D structure of UPD and vapor-deposited monolayers of Pb on Ag(111) and Au(111) are identical near full coverage.[3,7,8] In addition, it appears that vapor-deposited Bi/Ag(11) has the same uniaxial commensurate, rectangular structure as UPD Bi/Ag(111), although this is more tentative, since it is based on an analogy with Bi/Au(111).[13]

It is remarkable that the atomic structure of these metal layers is essentially equivalent in these two very different environments (e.g., under an electrolyte and in UHV). This shows that for the UPD of these heavy metals (Tl,Pb,Bi) on these smooth (111) surfaces (Ag and Au), the interaction between the solvent molecules and the adatoms does not influence the monolayer structure. Likewise, the structure is not significantly affected by interactions between the adatoms and any anions adsorbed on the UPD monolayer. It is important to determine if these conclusions can be generalized to other UPD systems.

Since we found that the structure of the UPD layer is not influenced by the solvent molecules, we will now consider the atomic interactions that are important in determining the structure of UPD (and vapor-deposited) Tl/Ag(111). The strongest interaction is that between the Tl adatoms and the substrate, since this bond strength is approximately equal to the Tl-Tl bond strength plus the UPD shift. Because this interaction is so strong, the Tl deposit forms a monolayer rather than bulk clusters; however, this interaction does not determine the structure within the monolayer. We conclude that the adatom-adatom interaction is the primary force that determines the crystallographic structure within the monolayer; this is deduced because the monolayer adopts a structure that is almost the same as that found in the closest-packed planes of bulk Tl and because the system is strongly incommensurate. Although the adatom-substrate interaction is strong, the corrugation or spatial variation in the adatom-substrate interaction is rather weak. It influences the structure only weakly by creating the local spatial modulation shown in Fig. 5(b) and discussed in Ref. 12. We have reached similar conclusions for UPD Tl on Au(111), Pb on Au(111) and Ag(111), and Bi on Ag(111).[42] To determine if these conclusions generalize to other UPD systems, it is important to investigate the structure of UPD layers on crystal faces other than (111).

Vapor-deposited Tl/Ag(111) certainly consists of *metallic* Tl atoms. From this and the fact that the structure of UPD Tl is essentially identical to the vapor-deposited layer, we conclude that the UPD monolayer is made up of zero-valent Tl atoms. This conclusion is consistent with previous voltammeteric evidence.[18] It is also supported by the reasonable agreement between the measured compressibility and that calculated for a 2D free-electron-gas model of a *metallic* monolayer (see Sec. V A). Since the adsorbed layer is metallic, the substrate-adsorbate bond is likely covalent, consistent with previous suggestions.[43–45]

D. Compression of the monolayer

A dramatic feature of the Tl monolayer is its large compression compared to bulk Tl. As described in Sec. VI A, this depends on potential, but even at the most positive potentials, the Tl-Tl near-neighbor spacing is compressed by more than 1.4%, and close to the Nernst potential, the compression becomes 3.0%. Note that a similar compression in bulk Tl (3% change in near-neighbor spacing) would require a pressure of about 50 000 atm. The UPD monolayers of Pb/Ag(111) (Ref. 9) and Pb and Tl on Au(111) (Ref. 42) are also found have similar compressions. These can all be understood within the framework of effective-medium theory,[46–49] which has been used to describe, for example, surface reconstructions and molecule-surface interaction potentials. In this theory the environment of an atom is modeled as a homogeneous electron gas and the binding energy of the atom is this environment (e.g., in a solid or at a surface) is related to the embedding energy of the atom in this homogeneous electron gas. The density of the electron

gas is called the embedding density and is an average of the electron density from the neighboring atoms in the system. Consequently, the embedding density is a monotonically decreasing function of atomic spacing.

First consider a simple bulk solid. The binding energy of an atom in this environment is the embedding energy plus an electrostatic term that accounts for the attraction between the "embedded" atom and the electron density tails from neighboring atoms. Both the embedding and electrostatic energies are functions of the embedding density. Since this density is related to the atomic spacing, the equilibrium atomic spacing is determined by the minimum in the binding energy as a function of embedding density.[46,47]

Now consider a free-standing monolayer, and notice that the coordination number of the atoms in this layer is less than that in the bulk solid. Thus, if the atomic spacing in the monolayer is the same as in the solid, the embedding density of the monolayer is less than the optimum density that gives the minimum binding energy. To reduce the binding energy, the embedding density must increase closer to the optimum density. This is achieved by a contraction or compression of the atomic spacing in the monolayer (compared to the bulk solid). For the more realistic case of an incommensurate monolayer on a substrate, the surface atoms of the substrate will contribute to the embedding density (i.e., they effectively increase the coordination number in the monolayer). Thus, the atomic spacing will be larger than in a free-standing monolayer but will still be smaller than bulk, since the coordination number is still smaller than in the solid. These ideas predict that the near-neighbor spacing in the bilayer should be closer to the bulk Tl spacing than in monolayer, since the average coordination number in the bilayer is closer to that in a solid (e.g., the first layer has neighbors above and below it). As shown in Sec. VII, this is precisely what is observed.

V. DEPENDENCE OF MONOLAYER STRUCTURE ON ANODIC- OR CATHODIC-SCAN DIRECTION

As can be seen in the CV of Tl on Ag(111) in Fig. 1, the current peaks for "deposition" (negative current) and "stripping" (positive current) do not occur at the same potential. Furthermore, these peaks are broadened with a FWHM of $\simeq 12$ mV. Both these features are generally observed for UPD systems and have been observed for scan rates as low as 0.2 mV/sec.[50] It is important to determine whether the offset between the deposition and stripping peaks is caused by kinetic effects or by actual structural differences in layers when the deposition potential is reached in an anodic (stripping or positive going) scan or cathodic (deposition or negative going) scan. Thus, the monolayer structure was investigated for a given potential, V, reached via anodic and cathodic scans. For the cathodic scans, the x-ray scattering measurements were conducted on monolayers formed by sweeping the potential from -100 mV to the desired potential V. To investigate the monolayer structure for anodic scans, the potential was first swept from -100 to -650 mV, the potential sweep direction reversed, and then the potential swept positively to the final potential V. The scan rate was always 2 mV/sec.

We found that at some potentials there were indications of small, initial changes in the position ($\simeq 0.05\%$ increase in $Q_{\|}$) and intensity ($\simeq 1-5\%$ increase) of the monolayer diffraction peak (which are currently being investigating). However, after about 30 min, the intensity and position of the Tl (10) diffraction peak did not change with time for as long as we waited (24 h). Moreover, the Tl (10) peaks were the same for both the anodic and cathodic scan directions. This is shown in Fig. 6, where radial and azimuthal diffraction scans are plotted for $V=-550$ mV when the final scan direction is anodic (solid triangles) and cathodic (open circles). In the diffraction data, the peaks for the anodic-scan direction are broader and less intense than for the cathodic-scan direction. However, this is just due to the time-dependent increase in the peak widths mentioned in Sec. IV; the anodic data were taken after the cathodic data. The important result is that the peak position in the radial scan [Fig. 6(a)] and the integrated intensities are the same for both the anodic and cathodic data. This is also readily apparent in Fig. 7, which shows the peak positions and integrated intensities at $V=-550$ mV for a sequence of anodic and cathodic scan directions (denoted A

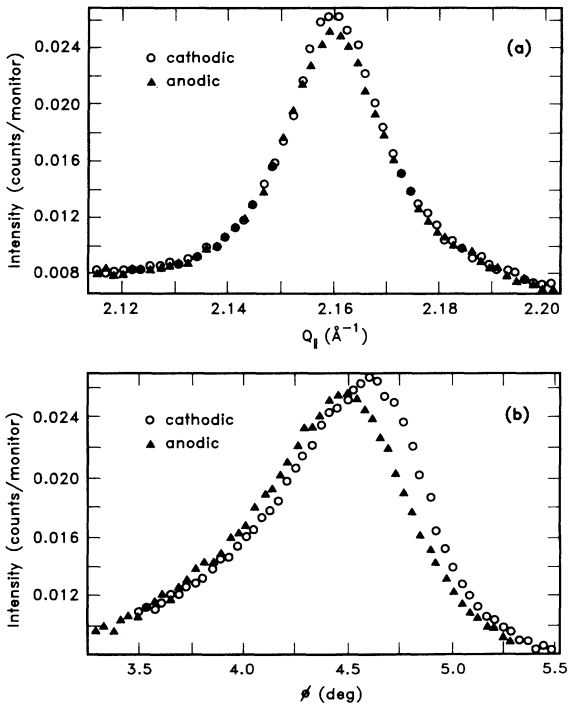

FIG. 6. Diffraction scans for Tl monolayers where the deposition potential of -550 mV (vs Ag/AgCl) is reached in an anodic or cathodic scan (solid triangles and open circles, respectively). Note that the diffracted intensity has been normalized to the monitor count rate and that $Q_z=0.15$ Å^{-1}. (a) Radial scans of the Tl (10) Bragg rod at the peak in the azimuthal scans ($\phi=4.45°$ and $4.6°$ for the anodic and cathodic data, respectively). (b) Azimuthal scans of the Tl (10) Bragg rod at $Q_{\|}=2.159$ Å^{-1}.

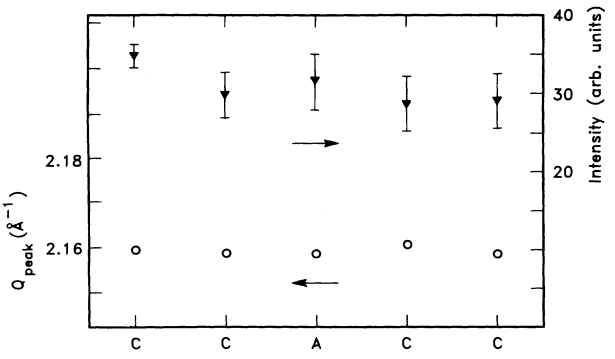

FIG. 7. The peak positions (open circles and left-hand scale) and integrated intensities (solid triangles and right-hand scale) for Tl monolayers where the electrode potential is $V=-550$ mV (vs Ag/AgCl) and is reached in anodic or cathodic scans (denoted *A* and *C*, respectively). The integrated intensities are from azimuthal scans and are in arbitrary units. They have been corrected for the increase in radial width with potential cycling (see Sec. IV). This was done by multiplication of the intensities in the azimuthal scans by the measured radial width. The errors for the peak positions are the size of the data points.

and *C*, respectively). Since both of these are the same, we conclude that the monolayer structure does not depend on whether the potential is reached in an anodic or cathodic scan. This behavior has also investigated at -500, -525, and -600 mV with identical results and conclusions.

These data show that for potentials between -500 and -600 mV (and probably lower) the monolayer is stable and is in thermodynamic equilibrium. This conclusion is consistent with voltammeteric and potential pulse experiments[18,19,21] that show the stripping characteristics of the monolayer are unaffected by holding the potential in this region for $\gtrsim 35$ min. Our data also suggest that the large UPD peaks in the CV (Fig. 1) are due to the discharge of the Tl cations as they undergo a first-order phase transition into the 2D close-packed, hexagonal solid phase (see Fig. 5) and that the peaks are not due to continuous adsorption.[19,51,52] The widths of the deposition and stripping peaks probably result from kinetic effects, and/or heterogeneity[53,54] of the Ag(111) substrate. The offset between the deposition and stripping peaks is likely due to kinetic effects and/or the influence of adsorbed SO_4^{2-} anions.

VI. DEPENDENCE OF MONOLAYER STRUCTURE ON POTENTIAL

In this section we describe our x-ray data for the dependence of the monolayer structure on electrode potential. In the potential range -500 to -680 mV (versus Ag/AgCl), the Tl monolayer has an incommensurate hexagonal structure that is compressed compared to the bulk metal and rotated about 4.5° from the Ag[01$\bar{1}$] direction. In this potential region, the monolayer exists in this single 2D phase, which is stable, but between -680 and -710 mV (i.e., the Nernst potential), the bilayer is the stable phase (see Sec. VII). Between -500 and -470 mV, the issue of phase stability is unclear (see below) and is the subject of further studies. The compression and rotation angle of the monolayer depend on electrode potential and these are described below.

A. Near-neighbor spacing (compressibility)

Figure 8 shows radial scans through the Tl (10) Bragg rod at three different electrode potentials. These show that with decreasing electrode potential the peak position shifts to larger $Q_{\parallel}$; this corresponds to a decrease in the near-neighbor spacing or a compression of the monolayer. We have also observed monolayer compression with decreasing electrode potential for Pb/Ag(111),[9] Bi/Ag(111),[13] and Tl and Pb/Au(111).[42] The changes in intensity and peak width that are apparent in Fig. 8 are due to the time-dependent changes in the monolayer diffraction discussed in Sec. IV. From this, it is evident that the data at -575 mV were taken first, the data at -650 mV sometime after that, and the data at -500 mV last.

The compression of the monolayer with decreasing electrode potential is readily understood: The chemical potential of the adatoms in the monolayer increases as the electrode potential decreases, because the potential drop across the metal-solution interface becomes more negative (i.e., the driving force to adsorb ions from solution increases). Since the chemical potential of the monolayer has increased, the monolayer free energy can be reduced by increasing the number of Tl adatoms on the Ag surface; this leads directly to the monolayer compression. The compression of UPD layers with decreasing potential

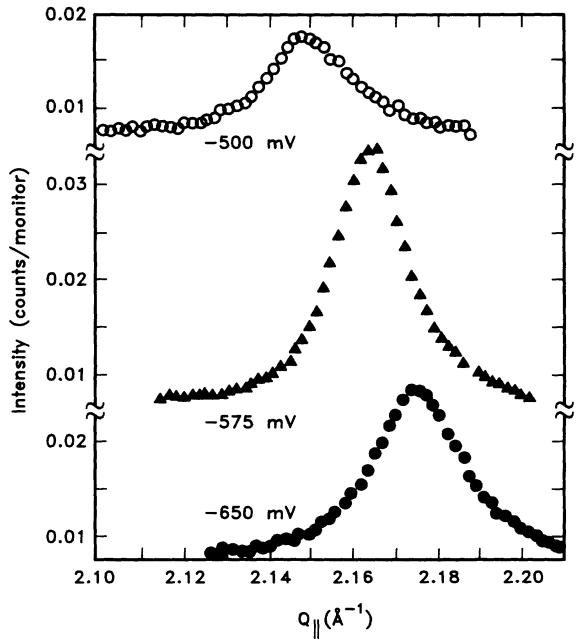

FIG. 8. Radial scans of the Tl(10) peak at -550 mV, -575 mV, and -650 mV. These show that the peak position shifts to larger $Q_{\parallel}$ with decreasing potential. The data at -575 mV were taken first, the data at -650 mV sometime after that, and the data at -500 mV last.

is completely analogous to vacuum experiments on the equilibrium adsorption of gases. There the chemical potential of the adsorbed layer is controlled by the vapor pressure of the gas, and an increase in the vapor pressure causes a compression of the adsorbed monolayer.[55–58]

Figure 9 shows the dependence of the near-neighbor distance a_{NN} on electrode potential. The datum at −477 mV (the most positive potential) may be due to diffraction from a metastable state. It was found that the diffraction peak at this potential disappeared slowly over about 2 h, even though the peak position was constant after a short initial time ($\simeq$15 min). This potential is very close to the potential where the Tl monolayer has been reported to be unstable, transforming into another phase after about 30 min.[18,19,21] We are continuing to investigate this apparently metastable behavior, as well as the nature of the structure that forms at this potential. Since the dependence of the near-neighbor spacing on potential shows some curvature, the data in Fig. 9 were least-squares-fitted to a quadratic function; the solid line shows the best fit. Note that the magnitude of the slope in Fig. 9 decreases with more negative electrode potentials or small a_{NN}; this is explained below.

We have previously demonstrated that the dependence of near-neighbor spacing a_{NN} on electrode potential can be used to determine the 2D isothermal compressibility of the monolayer, κ_{2D}.[3,9,13] We find that

$$\kappa_{2D} \equiv -\frac{1}{a}\left[\frac{\partial a}{\partial \Phi}\right]_T = \frac{\sqrt{3}a_{NN}}{Ze}\left[\frac{\partial a_{NN}}{\partial V}\right]_T , \quad (1)$$

where Φ is the 2D spreading pressure, a is the atomic area, Z is the number of electrons transferred per atom deposited, and V is the electrode potential.[3,9,13] It is important to note that this relationship requires chemical and thermal equilibrium between the monolayer and the adsorbing species. For metallic adsorbates this is readily achievable in electrochemical environments (where the adsorbing species are ions in solution), but it is almost impossible to achieve chemical equilibrium in vacuum (where the adsorbing species are free metal atoms).

Using Eq. (1) and the derivative of the best-fit quadratic function to the data (shown by the line in Fig. 9), we calculate that for Tl/Ag(111) κ_{2D} varies linearly with potential from 2.2±0.15 Å^2/eV at −480 mV to 0.90±0.10 Å^2/eV at −650 mV. The average compressibility is $\kappa_{2D}=1.54\pm0.10$ Å^2/eV, which is about the same as previously found for Tl/Au(111), Bi/Ag(111), and Pb on Au(111) and Ag(111).[3,9,13,42] The decrease in the compressibility of Tl/Ag(111) with more negative electrode potentials or smaller near neighbor spacing is expected: As the atomic spacing decreases, the adatom-adatom repulsive force becomes increasingly stronger, and this makes it increasingly difficult to pack the adatoms closer together. For Tl and Pb on Au(111), a similar decrease in compressibility is observed as the potential becomes negative.

For most bulk metals the compressibility is dominated by the electron compressibility,[59] and hence, a similar domination is expected for metal monolayers. Using a 2D free-electron-gas model of the compressibility,[3,9,42,59] we estimate $\kappa_{2D}=0.44$ Å^2/eV. This is in reasonable agreement with our experiment; in fact, the agreement is as good as that found for a three-dimensional free-electron gas and bulk Tl. It would be interesting to see if a more realistic value of κ_{2D} could be predicted with a more sophisticated model of Tl on Ag(111), such as an embedded-atom model.[60]

B. Rotation angle

The rotation angle Ω is also dependent on electrode potential, but this behavior cannot be accurately quantified, because of the irreversible decrease in Ω with potential cycling discussed in Sec. IV. However, the qualitative behavior can be determined. This is shown in Fig. 10, where Ω is plotted as a function of potential for two Ag(111) substrates. The lines and arrows show how the potential was changed. For each potential the electrochemical cell was inflated and one or more complete potential cycles conducted (e.g., the potential was swept positively to −100 mV and then negatively to the new potential). These data show the irreversible decrease in Ω with cycling described in Sec. IV; they also show that Ω depends on potential and that for the monolayer, Ω increases with increasing potential or decreasing near-neighbor spacing (for example, Ω at −550 mV is larger than at −650 mV even when the data at −550 mV are obtained subsequent to those obtained at −650 mV).

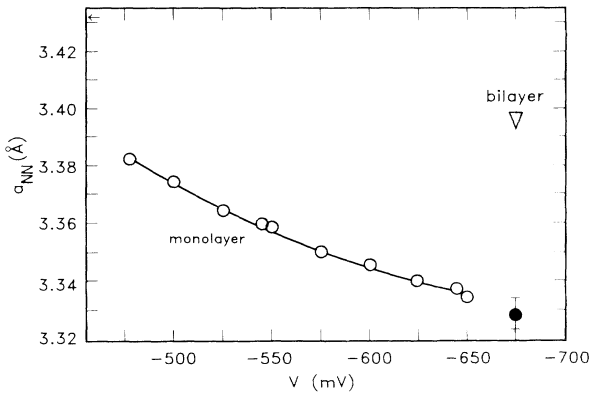

FIG. 9. Dependence of the Tl layer near-neighbor distance on the electrode potential, V (vs Ag/AgCl). The triangle is for the bilayer, whereas the solid circle is for the metastable monolayer phase that coexists with the bilayer (see Sec. VII). Except for this datum, the errors are the size of the data points. The data are plotted as a function of decreasing potential, since a change in chemical potential of the monolayer is proportional to the negative of the change in electrode potential. The line is the least-squares fit of a quadratic ($a_{NN}=C_2V^2+C_1V+C_0$) to the data with the result $C_0=3.7101$, $C_1=9.959\times10^{-4}$, and $C_2=6.471\times10^{-7}$. (a_{NN} is in Å and V is in mV.) The arrow marks the "average" near-neighbor spacing for bulk Tl. Since bulk Tl is hexagonal close packed (hcp), there are two "near-neighbor" spacings that are almost the same. The average spacing (3.432 Å) was calculated by setting the volume of the hcp unit cell for Tl equal to the volume of a (hypothetical) face-centered-cubic cell, which has a unique near-neighbor spacing.

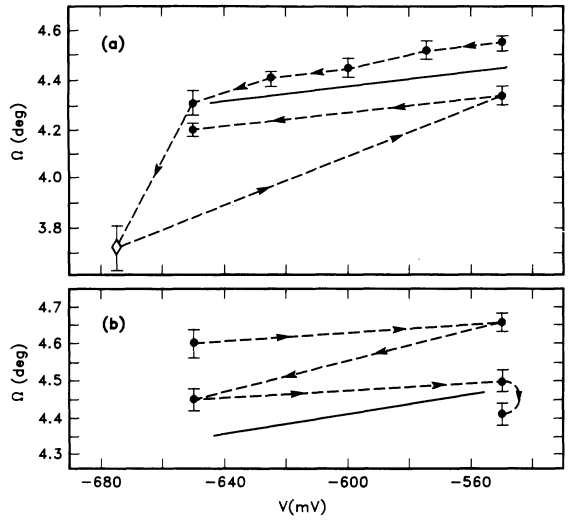

FIG. 10. Dependence of rotation angle Ω on electrode potential V (vs Ag/AgCl). The dashed lines and associated arrows show the order in which the data were taken. The circles are for the monolayer, whereas the diamond is for the bilayer. Data from two Ag(111) substrates are shown [(a) and (b), respectively]. The solid lines indicate our estimate of the average slope.

From Fig. 10, we estimate a slope of $d\Omega/dV = 1.4 \pm 0.6$ deg/V for the monolayer, as indicated by the solid lines.

Novaco and McTague (NM) have developed a model to describe the dependence of the rotation angle on the near-neighbor spacing.[61,62] The periodic potential of the substrate creates a small spatial modulation in the position of the adatoms [see Fig. 5(b)], which allows the adatoms to sit closer to the low-energy sites of the substrate. The rotation results because the energy of the adsorbed layer is lower when the monolayer rotates away from a high-symmetry direction of the substrate (i.e., it takes less energy to create a shear wave than a compressive wave).[61,62] The NM model explains the dependence of rotation angle on near-neighbor spacing for incommensurate monolayers of inert gases physically adsorbed on graphite[63] and on metals[64] and for incommensurate monolayers of alkali-metal atoms chemisorbed on metals[65,66] and on graphite.[67] It is useful to compare the NM model to our data, since such a comparison has not been made for metallic overlayers on hexagonal substrates, and since in none of the previous observations has the monolayer structure been close to a commensurate (1×1) structure on a hexagonal substrate. However, a word of caution is in order: it is not clear that all the assumptions of the NM model are satisfied for Tl/Ag(111) (see Ref. 12 for discussion). Nor are our data good enough to expect quantitative agreement with the model, because of the irreversible decrease of Ω with potential cycling (see Sec. IV).

In the NM model,[61,62] the monolayer longitudinal and transverse sound velocities (C_L and C_T, respectively) are important parameters. Unfortunately, these are unknown for Tl/Ag(111). In Ref. 12, we estimated these quantities by modeling the monolayer as a thin plate of bulk Tl with the (00.1) direction normal to the plate; this model and the bulk elastic constants were then used to calculate the in-plane values of Young's modulus and Poisson's ratio,[68–70] and from these, C_L and C_T were calculated. We found $\eta \equiv (c_L/c_T)^2 - 1 \simeq 2.75$. Because of the uncertainty of our assumptions, the error in this estimate is unclear, but we (conservatively) expect that η falls between about 2 (the value for a 2D Cauchy solid) and about 3.5. This uncertainty is large enough that one should not anticipate quantitative agreement between our data and the absolute rotation angles calculated with the NM model. In view of this and the cautions noted in the preceding paragraph, the best to be expected is qualitative agreement, and indeed, this is observed. For $2 < \eta < 3.5$ and for our observed range of near-neighbor spacing ($a_{NN} = 3.38$–3.33 Å), the NM model gives $\Omega \sim 4.3°$–$6.3°$. Figure 10 shows that, for the Tl monolayer, $\Omega \sim 4.2°$–$4.7°$.

The derivative of the rotation angle with respect to the near-neighbor distance, $d\Omega/da_{NN}$ depends less sensitively on η than the absolute rotation angle. Furthermore, the NM model predicts that $d\Omega/da_{NN}$ should be essentially constant over our measured range of near-neighbor spacing. Thus, it is also useful to compare a calculation of $d\Omega/da_{NN}$ to the data. Figure 10 shows $d\Omega/dV = 1.4 \pm 0.6$ deg/V, and since the average slope in Fig. 9 is $da_{NN}/dV = 0.27$ Å/V, we find $d\Omega/da_{NN} = 5.3 \pm 2.3$ deg/Å. With the NM model, the slope is calculated as $d\Omega/da_{NN} = 7.6$, 10.0, and 11.3 deg/Å, for $\eta = 2$, 2.75, and 3.5, respectively. Thus, the derivative predicted with the NM model is also in reasonable qualitative agreement with our data.

Our data for the dependence of the rotation angle on near-neighbor spacing agrees qualitatively (indeed, almost semiquantitatively) with the NM model, which is the most to be expected, considering all the uncertainties. This is significant because there have been no tests of the NM model for *metallic* adsorbed layers or for overlayers on hexagonal substrates where the structure is close to a (1×1) commensurate lattice. A better test will require obtaining a better value for η and understanding and eliminating the cause of the irreversible decrease of Ω (presumably, adsorption of trace levels of organics, see Sec. IV B).

VII. BILAYER STRUCTURE FOR Tl/Ag(111)

Two layers of Tl (a bilayer) can be deposited by UPD on Ag(111), but not on Au(111).[30,71] To understand this difference, it is first important to determine the structure of the bilayer phase. This structure is also of interest in its own right, since the two Tl layers may be either mutually commensurate[18] or incommensurate.[27] Our experiments are described in detail in a separate publication, where we report measurements of the intensities along the Tl (10) and (11) Bragg rods of the bilayer.[42] For completeness, the results of these measurements are briefly described here. We find that the second Tl layer is commensurate with the layer beneath it and the second-layer atoms are positioned in the threefold-hollow sites of the

bottom Tl layer. The spacing between the layers is about 2.85 Å, 0.1 Å larger than for bulk Tl, and there is more disorder in the bilayer phase than in the monolayer. Although the Tl layers in the bilayer are mutually commensurate, the entire bilayer structure is incommensurate with the Ag(111) substrate. The near-neighbor spacing in the bilayer is 3.397 Å, which is significantly larger and closer to bulk Tl than in the monolayer (see Fig. 9). Since the average coordination number in the bilayer is larger than in the monolayer, this is just what is expected from effective-medium theory (see Sec. IV D).

The rotation angle Ω for the bilayer is about 3.9°, which is smaller than that for the monolayer, even though a_{NN} is larger (see Figs. 9 and 10). Thus, the rotation angle of the bilayer breaks the trend observed in the monolayer: upon going from the monolayer to the bilayer, $d\Omega/da_{NN}$ is negative, which is opposite to that observed for the monolayer and that suggested by the NM model.[61,62] This probably results because there is a large difference in the elastic constants (and hence the sound velocities) between the bilayer and monolayer, or perhaps, because anharmonic interactions are more important in the bilayer (the NM model assumes harmonic interactions between adatoms).

At electrode potentials where the bilayer phase exists (see Fig. 1), we observe diffraction peaks from both the bilayer and phase with a more compressed structure. The near-neighbor spacing for the compressed phase is about 3.33 Å (see Fig. 9). This spacing is consistent with an extrapolation of the near-neighbor spacings in the monolayer phase. It is found that the intensity of the peak from the compressed phase decreases with time (several hours). This suggests that the compressed phase is a metastable monolayer phase and that at these potentials, there is transient coexistence between this metasable monolayer and the stable bilayer phase. The changes with time are then due to the kinetics of a monolayer-to-bilayer phase transformation.

Fleischmann and Mao have also used *in situ* x-ray diffraction to study Tl bilayers deposited on roughened Ag electrodes.[27] A modulation technique was used; data were taken at a potential where the layer was not adsorbed on the electrode and were subtracted from data taken at a potential where the Tl bilayer was adsorbed. The major feature observed by Fleischmann and Mao was an enhancement of the Ag(111) diffraction peak, which they attributed to the presence of a Tl (11) surface diffraction peak at the same position as the Ag(111) diffraction peak. This feature was interpreted as resulting from a commensurate first (or bottom) layer of Tl on the (111) facets of the roughened Ag electrode. However, such a structure will not produce Tl (11) peaks at the Ag(111) positions and also requires an unreasonably large compression in the first layer (19%). Two less defined features were also observed[27] and were attributed to diffraction from a top layer with an oblique lattice that is incommensurate with the bottom layer.

The structure for the Tl bilayer that was proposed by Fleischmann and Mao[27] does not explain their data and disagrees with our results. Here we propose an alternative explanation of their data. The enhancement of the Ag(111) peak probably results because the Ag(111) d spacing (2.36 Å) is comparable to the spacing between the top and bottom Tl layers ($\simeq$2.85 Å) and the spacing between the bottom Tl layer and the Ag surface ($\simeq$3 Å).[12] Thus, the deposition of the Tl bilayer effectively increases the thickness of the Ag(111) crystallites and this results in an increase in the diffracted intensity near the Ag(111) peak. A similar effect has been observed for Ar and N_2 physically adsorbed on Grafoil (a graphite powder).[72,73] The more poorly defined features observed by Fleischmann and Mao[27] correspond to d spacings of 2.57 and 2.89 Å. These are close to the bulk Tl(101) and Tl bilayer (10) d spacings (2.63 and 2.94 Å, respectively), and we speculate that these observed features are due to diffraction from bulk Tl and the bilayer.

VIII. SUMMARY AND CONCLUSIONS

In situ surface x-ray scattering has been used to investigate UPD layers of Tl on Ag(111). We have considered this to be a prototypical UPD system and have investigated it in some detail with interesting and important results. In this paper we have described the atomic structure, the thermodynamic stability, and the dependence of the structure on electrode potential. Between potentials of −475 and −680 mV (versus Ag/AgCl), the Tl deposit forms an incommensurate, hexagonal monolayer that is compressed relative to bulk Tl by 1.4–3.0% and rotated from the Ag [01$\bar{1}$] direction by Ω=4°–5°. At −550 mV, the in-plane and vertical root-mean-square displacement amplitudes of the monolayer are 0.36±0.1 and 0.46±0.1 Å, respectively. The equivalence of the atomic structure for UPD and vapor-deposited[41] Tl/Ag(111) suggests that the UPD layer consists of zero-valent Tl adatoms, which agrees with electrochemical voltammeteric evidence.[18] Furthermore, this equivalence shows that the solvent-adatom interactions do not influence the monolayer structure. That the monolayer structure is about the same as the closest-packed planes of the bulk Tl indicates the adatom-adatom interactions are the primary forces determining the structure for this UPD system. The monolayer structure is only weakly influenced by adatom-substrate interactions, which create the local spatial modulation of the adatom positions.[12]

The compression of the monolayer (compared to bulk Tl) is explained in terms of effective-medium theory.[46–49] In the Tl monolayer, the coordination is less than in bulk Tl and hence if the atomic spacing in the monolayer is the same as in bulk, the electron density in the monolayer will be less than the optimum density. For the electron density to increase closer to the optimum density, the monolayer must contract or compress compared to the bulk solid. These ideas also explain why the near-neighbor spacing in the bilayer is closer to the bulk Tl spacing than in the monolayer.

Between −500 and −680 mV, the monolayer is stable for at least 24 h (our longest observation time), and the monolayer structure does not depend on whether the potential is reached in an anodic (stripping) or cathodic (deposition) scan. This shows that the monolayer is in thermodynamic equilibrium and that the offset and ob-

served width of the peaks in the cyclic voltammograms are due to kinetics, the influence of adsorbed anions, and/or substrate heterogeneity. These observations also indicate that the large UPD peaks are due to a first-order phase transition into the close-packed hexagonal, 2D solid phase.

The in-plane spacing between Tl adatoms decreases with decreasing electrode potential. This results because a decrease in the electrode potential corresponds to an increase in the monolayer chemical potential, which favors the adsorption of more Tl to minimize the free energy. From our data, the 2D compressibility (κ_{2D}) of the Tl monolayer can be calculated, since the monolayer is in chemical equilibrium with the adsorbing species. We find that κ_{2D} varies from 2.2 ± 0.15 (at -480 mV) to 0.90 ± 0.10 Å^2/eV (at -650 mV) and has an average value of $\kappa_{2D}=1.54\pm0.10$ Å^2/eV. This is similar to previously measured compressibilities of UPD monolayers[3,9,13] and is in reasonable agreement with theoretical estimates using a 2D free-electron-gas model (0.44 Å^2/eV). The rotation angle Ω depends on the electrode potential and adatom spacing, but irreversibly decreases with potential cycling, and we speculate that this is due to the adsorption of trace impurities. Despite this irreversibility, the dependence of Ω on adatom spacing qualitatively agrees with Novaco-McTague model.[61,62]

Between -680 and -710 mV (the bulk deposition potential), the Tl deposit forms a bilayer with an incommensurate, hexagonal structure. For the bilayer, the compression (compared to bulk Tl) and rotation (from Ag [01$\bar{1}$]) are 1.0% and 3.9°, respectively, and are less than for the monolayer.[42]

ACKNOWLEDGMENTS

We thank Jean Jordan-Sweet and Brian Stephenson for their assistance with beam line X20A, Ian Robinson for lending us his Soller slits, and Dave Wiesler for useful discussions. This work was partially supported by the Office of Naval Research. It was performed at the National Synchrotron Light Source, Brookhaven National Laboratory, which is supported by the U.S. Department of Energy, Division of Materials Sciences and Division of Chemical Sciences.

[1]D. Kolb, M. Przasnyski, and H. Gerischer, J. Electroanal. Chem. **54**, 25 (1974).

[2]D. M. Kolb, in *Advances in Electrochemistry and Electrochemical Engineering,* edited by H. Gerischer and C. W. Tobias (Wiley, New York, 1978), Vol. 11, p. 125.

[3]M. F. Toney and O. R. Melroy, in *Electrochemical Interfaces: Modern Techniques for In-Situ Interface Characterization,* edited by H. D. Abruna (VCH Verlag Chemical, Berlin, 1991), p. 57.

[4]M. F. Toney, in *The Application of Surface Analysis Methods to Environmental/Materials Interactions,* edited by D. R. Baer, C. R. Clayton, and G. D. Davis (The Electrochemical Society, Pennington, NJ, 1991), p. 200.

[5]O. R. Melroy, M. G. Samant, G. L. Borges, J. G. Gordon, L. Blum, J. H. White, M. J. Albaretti, M. McMillan, and H. D. Abruna, Langmuir **4**, 728 (1988).

[6]M. G. Samant, G. L. Borges, J. G. Gordon, L. Blum, and O. R. Melroy, J. Am. Chem. Soc. **109**, 5970 (1987).

[7]M. G. Samant, M. F. Toney, G. L. Borges, L. Blum, and O. R. Melroy, Surf. Sci. **193**, L29 (1988).

[8]M. G. Samant, M. F. Toney, G. L. Borges, L. Blum, and O. R. Melroy, J. Phys. Chem. **92**, 220 (1988).

[9]O. R. Melroy, M. F. Toney, G. L. Borges, M. G. Samant, J. B. Kortright, P. N. Ross, and L. Blum, Phys. Rev. B **38**, 10 962 (1988).

[10]M. F. Toney and O. R. Melroy, in *Synchrotron Radiation in Materials Research,* edited by R. Clarke, MRS Symposia Proceedings No. 143 (Materials Research Society, Pittsburgh, 1989), p. 37.

[11]O. R. Melroy, M. F. Toney, G. L. Borges, M. G. Samant, J. B. Kortright, P. N. Ross, and L. Blum, J. Electroanal. Chem. **258**, 403 (1989).

[12]M. F. Toney, J. G. Gordon, L. S. Kau, G. Borges, O. R. Melroy, M. G. Samant, D. G. Wiesler, D. Yee, and L. B. Sorensen, Phys. Rev. B **42**, 5594 (1990).

[13]M. F. Toney, J. G. Gordon, M. G. Samant, G. L. Borges, D. G. Wiesler, D. Yee, and L. B. Sorensen, Langmuir **7**, 796 (1991).

[14]M. J. Bedzyk, G. M. Bommarito, M. Caffrey, and T. L. Penner, Science **248**, 52 (1990).

[15]B. Ocko, J. Wang, A. Davenport, and H. Isaacs, Phys. Rev. Lett. **65**, 1466 (1990).

[16]C. A. Melendres, H. You, V. A. Maroni, Z. Nagy, and W. Yun, J. Electroanal. Chem. **297**, 549 (1991).

[17]H. You, C. A. Melendres, Z. Nagy, V. A. Maroni, W. Yun, and R. M. Yonco, Phys. Rev. B (to be published).

[18]H. Siegenthaler, K. Juttner, E. Schmidt, and W. J. Lorenz, Electrochim. Acta **23**, 1009 (1978).

[19]K. Juttner and H. Siegenthaler, Electrochim. Acta **23**, 971 (1978).

[20]G. Staikov, K. Juttner, W. J. Lorenz, and E. Budevski, Electrochim. Acta **23**, 319 (1978).

[21]E. Schmidt and H. Siegenthaler, J. Electroanal. Chem. **150**, 59 (1983).

[22]V. D. Jovic, B. M. Jovic, and A. R. Despic, J. Electroanal. Chem. **288**, 229 (1990).

[23]A. Bewick and B. Thomas, J. Electroanal. Chem. **65**, 911 (1975).

[24]D. A. Koos, V. L. Shannon, and G. L. Richmond, J. Phys. Chem. **94**, 2091 (1990).

[25]T. E. Furtak, J. Miragliotta, and G. M. Korenowski, Phys. Rev. B **35**, 2569 (1987).

[26]J. Miragliotta and T. E. Furtak, Surf. Interface Anal. **14**, 53 (1989).

[27]M. Fleischmann and B. W. Mao, J. Electroanal. Chim. **247**, 297 (1988).

[28]E. D. Specht, A. Mak, C. Peters, M. Sutton, R. J. Birgeneau, K. L. D'Amico, D. E. Moncton, S. E. Nagler, and P. M. Horn, Z. Phys. B **69**, 347 (1987).

[29]W. R. Busing and H. A. Levy, Acta Crystallogr. **22**, 457 (1967).

[30]W. J. Lorenz, H. D. Hermann, N. Wuthrich, and F. Helbert,

J. Electrochem. Soc. **121**, 1167 (1974).
[31]M. F. Toney, D. G. Wiesler, D. Yee, and L. B. Sorensen (unpublished).
[32]J. A. Ibers and W. C. Hamilton, *International Tables for X-Ray Crystallography* (Kynoch, Birmingham, England, 1974), Vol. IV.
[33]M. S. Altman, P. J. Estrup, and I. K. Robinson, Phys. Rev. B **38**, 5211 (1988).
[34]I. K. Robinson, Aust. J. Phys. **41**, 359 (1988).
[35]Here *b* is the width of Lorentzian squared. See Ref. 12 for the precise definition of *b*.
[36]C. H. MacGillavry, G. D. Rieck, and K. Lonsdale, *International Tables for X-Ray Crystallography* (Kynoch, Birmingham, England, 1962), Vol. III.
[37]A. Zangwill, *Physics at Surfaces* (Cambridge University Press, Cambridge, 1988).
[38]The effect of instrumental resolution has been removed from the peak widths.
[39]B. E. Warren, *X-Ray Diffraction* (Addison-Wesley, Reading, MA, 1969).
[40]K. Kern, P. Zeppenfeld, R. David, R. L. Palmer, and G. Comsa, Phys. Rev. Lett. **57**, 3187 (1986).
[41]K. J. Rawlings, M. J. Gibson, and P. J. Dobson, J. Phys. D **11**, 2059 (1978).
[42]M. F. Toney, J. G. Gordon, G. Borges, D. G. Wiesler, D. Yee, and L. B. Sorensen (unpublished).
[43]C. Mayer, K. Juttner, and W. J. Lorenz, J. Appl. Electrochem. **9**, 161 (1979).
[44]J. W. Schultze and K. J. Vetter, J. Electroanal. Chem. **44**, 63 (1973).
[45]J. W. Schultze and F. D. Koppitz, Electrochim. Acta **21**, 327 (1976).
[46]K. W. Jacobsen, J. K. Nørskov, and M. J. Puska, Phys. Rev. B **35**, 7423 (1987).
[47]K. W. Jacobsen, Comments Condensed Matter Phys. **14**, 129 (1988).
[48]K. W. Jacobsen and J. K. Nørskov, in *The Structure of Surfaces II*, edited by J. F. van der Veen and M. A. Van Hove (Springer-Verlag, Berlin, 1988), p. 118.
[49]J. K. Nørskov, J. Chem. Phys. **90**, 7461 (1989).
[50]J. N. Jovicevic, V. D. Jovic, and A. R. Despic, Electrochim. Acta **29**, 1625 (1984).
[51]K. Juttner, G. Staikov, W. J. Lorenz, and E. Schmidt, J. Electroanal. Chem. **80**, 67 (1977).
[52]K. Juttner and W. J. Lorenz, Z. Phys. Chem. **122**, 163 (1980).
[53]J. G. Dash and R. D. Puff, Phys Rev. B **24**, 295 (1981).
[54]R. E. Ecke, J. G. Dash, and R. D. Puff, Phys. Rev. B **26**, 1288 (1982).
[55]C. G. Shaw and S. C. Fain, Surf. Sci. **83**, 1 (1979).
[56]C. G. Shaw and S. C. Fain, Surf. Sci. **91**, L1 (1980).
[57]L. W. Bruch and J. M. Phillips, Surf. Sci. **91**, 1 (1980).
[58]J. Unguris, L. W. Bruch, E. R. Moog, and M. B. Webb, Surf. Sci. **109**, 522 (1981).
[59]N. W. Ashcroft and N. D. Mermin, *Solid State Physics* (Saunders College, Philadelphia, 1976).
[60]M. S. Daw and M. I. Baskes, Phys. Rev. B **29**, 6443 (1984).
[61]J. P. McTague and A. D. Novaco, Phys Rev. B **19**, 5299 (1979).
[62]A. D. Novaco and J. P. McTague, Phys. Rev. Lett. **38**, 1286 (1977).
[63]C. G. Shaw, S. C. Fain, and M. D. Chinn, Phys. Rev. Lett. **41**, 955 (1978).
[64]K. Kern, Phys. Rev. B **35**, 8265 (1987).
[65]D. L. Doering and S. Semancik, Phys. Rev. Lett. **53**, 66 (1984).
[66]J. Cousty and R. Riwan, Surf. Sci. **204**, 45 (1988).
[67]N. J. Wu, Z. P. Hu, and A. Ignatiev, Phys. Rev. B **43**, 3805 (1991).
[68]J. F. Nye, *Physical Properties of Crystals* (Oxford University Press, London, 1957).
[69]G. Simmons and H. Wang, *Single Crystal Elastic Constants and Calculated Aggregate Properties: A Handbook* (MIT Press, Cambridge, MA, 1971).
[70]L. D. Landau and E. M. Lifshitz, *Statistical Physics* (Addison-Wesley, Reading, MA, 1969).
[71]J. W. Schultze and D. Dickertmann, Surf. Sci. **54**, 489 (1976).
[72]J. K. Kjems, L. Passell, H. Taub, J. G. Dash, and A. D. Novaco, Phys. Rev. B **13**, 1446 (1976).
[73]H. Taub, K. Carneiro, J. K. Kjems, L. Passell, and J. P. McTague, Phys. Rev. B **16**, 4551 (1977).

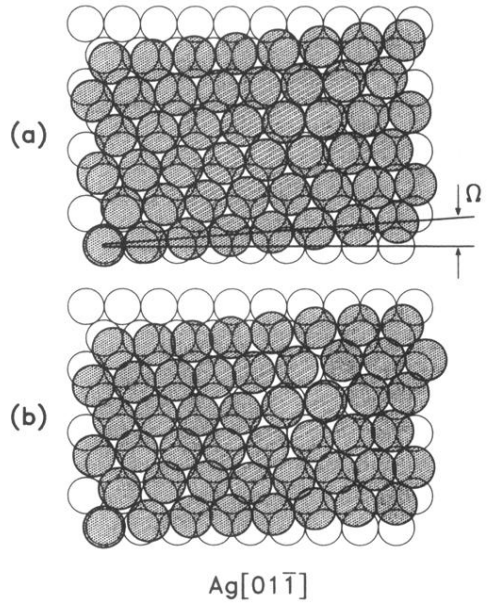

FIG. 5. Schematic real-space representation of one domain of monolayer Tl on Ag(111). The rotation angle between the Ag and Tl lattices is $\Omega = 4.5°$ and the average near-neighbor spacing of the Tl monolayer is 3.36 Å. The open circles represent atoms in the Ag(111) surface and the solid circles represent the Tl atoms; the lower leftmost adatom is arbitrarily positioned above a Ag atom. (a) The (hypothetical) unmodulated or average structure. (b) The modulated monolayer. The adatoms positions are calculated as described in Ref. 12.